Novel Electromagnetic Interference Shielding Effectiveness in the Microwave Band of Magnetic Nitrile Butadiene Rubber/Magnetite Nanocomposites

A. A. Al-Ghamdi,[1] Omar A. Al-Hartomy,[1,2] F. Al-Salamy,[3,4] Attieh A. Al-Ghamdi,[5] E. H. El-Mossalamy,[6] A. M. Abdel Daiem,[1,7] Farid El-Tantawy[8]

[1]*Faculty of Science, Department of Physics, King Abdulaziz University, Jeddah, P. O. 80203, Jeddah 21589, Saudi Arabia*
[2]*Faculty of Science, Department of Physics, University of Tabuk, Tabuk, Saudi Arabia*
[3]*Faculty of Science Department of Mathematics, University of Tabuk, Tabuk, Saudi Arabia*
[4]*Faculty of Science Department of Mathematics, King Abdulaziz University, Jeddah, P. O. 80203, Jeddah 21589, Saudi Arabia*
[5]*King Abdulaziz City for Science and Technology, Electronics Communications and Photonics Program, Riyadh, Kingdom of Saudi Arabia*
[6]*Faculty of Science, Chemistry Department, King Abdulaziz University, Jeddah, P. O. 80203, Jeddah 21589, Saudi Arabia*
[7]*Faculty of Science, Department of Physics, Zagazig University, Zagazig, Egypt*
[8]*Faculty of Science, Department of Physics, Suez Canal University, Ismailia, Egypt*

Received 17 June 2011; accepted 13 October 2011
DOI 10.1002/app.36371
Published online 29 January 2012 in Wiley Online Library (wileyonlinelibrary.com).

ABSTRACT: A novel nitrile butadiene rubber (NBR)/magnetite (Fe_3O_4) nanocomposite for electromagnetic interference (EMI) shielding at microwave frequency was successfully fabricated. The structural features of as-synthesized magnetite and NBR/Fe_3O_4 were examined by X-ray diffraction, field emission scanning electron microscopy, transmission electron microscopy, and energy-dispersive X-ray spectroscopy. The number of elastically effective chains, volume fraction of rubber, interparticle distance among conductive sites, polymer–filler interaction, and porosity of the nanocomposites were evaluated. The mechanical properties, including the tensile strength, elongation at break, and hardness, of the composites were measured. The static electrical properties, such as the electrical conductivity, carrier mobility, and number of charge carriers, as a function of magnetite content were evaluated. The interrelation between the electrical conductivity, shielding effectiveness (SE), dielectric constant, and skin depth of the composites are discussed. Finally, the EMI SE versus frequency was tested. The results reveal that an SE of 28–91 dB against EMI in the 1–12 GHz range depended on the loading of the conducting magnetite within the NBR matrix. Accordingly, these nanocomposites may used in the field of microwave absorption devices. © 2012 Wiley Periodicals, Inc. J Appl Polym Sci 125: 2604–2613, 2012

Key words: mechanical properties; microstructure; nanocomposites; rubber; TEM

INTRODUCTION

As the microwave business grows and with the rapid development of electronic and communications technology, electromagnetic radiation has emerged as a new form of contamination in modern communities and has been listed as the third biggest pollutant.[1] Recently, several electronic devices with high frequencies, including satellite communication, automobile collision prevention radar, accident surveillance of railroads, cellular phones, and wireless local area networks, have been developed and applied.[2–6] The electromagnetic waves produced from some electronic devices have an adverse influence on the performance of other equipment and may cause malfunctions in medical equipment; industry robots cause harm to the human body and become a public nuisance.[7–9] Therefore, to alleviate these troubles, the development of electromagnetic interference (EMI) shielding materials for microwave and millimeter waves are receiving increasing attention. Metal EMI shielding materials, such as steel, copper, and aluminum, have the shortcomings of heavy weight, corrosion, and physical rigidity.[10] This can be solved to a great extent by replacing conventional metal-based EMI shielding materials with electrically conducting polymer nanocomposites because of their light weight, resistance to correction, flexibility, processing advantages, and other advantages.[11] In fact, most polymer matrices in composites are typically

Correspondence to: F. El-Tantawy (faridtantawy@yahoo.com).

Contract grant sponsor: University of Tabuk (to A.A.A.-G., O.A.A.-H., F.A.-S., and F.E.-T.).

electrically insulating, so they are not able to provide EMI shielding.[12] The EMI shielding efficiency of a composite material depends on many factors, including the filler's intrinsic conductivity, dielectric constant, aspect ratio of the filler (length-to-diameter), volume fraction of the filler, polarities of the filler and matrix, and extent of the filler reinforcement.[13–15] Magnetite (Fe_3O_4) nanoparticles have recently attracted great attention because of their valuable properties, including a high electrical conductivity, use in information storage, medical care, magnetic sensing, and ferrofluids, low toxicity, high Curie temperature, and nearly full spin polarization at room temperature; these properties have great potential for applications in giant magnetoelectronic, spin-valve devices.[16] Such fascinating properties have inspired interest the use of magnetite nanoparticles as fillers in polymer composite systems to obtain ultralight structural materials with enhanced electrical, thermal, and mechanical characteristics. To this point, there has been no report in the open literature on nitrile butadiene rubber (NBR)-reinforced magnetite (Fe_3O_4) nanoparticles for EMI shielding at microwave frequency. The aim of this study was to fabricate a new magnetic nanocomposites based on NBR and magnetite for EMI shielding at microwave frequency. The interrelations among the network structure and EMI shielding at high frequency for the NBR/magnetite nanocomposites were investigated in detail.

EXPERIMENTAL

Synthesis of magnetite (Fe_3O_4) nanoparticles

All of the reagents were of analytical purity and were used directly without further purification. Synthesis was carried out according to the following procedure: 0.025 mol of ferric chloride hexahydrate ($FeCl_3{\cdot}6H_2O$) was dissolved in 15 mL of deionized water with 0.07 g of $Na_2C_2O_4$ and 15 mL of ethylene glycol with strong magnetic stirring at room temperature for 30 min to get a clear solution. The clear solution was transferred into a Teflon-lined, stainless steel autoclave with a 100-mL capacity. The autoclave was sealed and heated at 200°C for 10 h. After the heating treatment, the autoclave was naturally cooled down to room temperature. The black products were collected by centrifugation, washed three times with deionized water and absolute ethanol, and then dried naturally in air. Calcination was performed at 325°C for 3 h in a furnace.

Nanocomposite preparation

The NBR used in this study was a commercial grade supplied by Alexandria Trade Rubber Co. [Alexandria, Egypt, density = 0.98 g/cm^3, acrylonitrile content = 34%, Mooney viscosity $ML_{(1+4)}$ at 100°C = 50 (ASTM D 1646), average molecular weight = 163,376, glass temperature of about 36°C]. The as-synthesized magnetite nanoparticles (particle size = 6 nm) were used as a conducting and reinforcing filler. Other compounding ingredients, including stearic acid (accelerator), zinc oxide (activator), dioctyl phthalate (DOP) plasticizer, dibenzthiazyl disulfide (MBTS) and tetramethyl thiuram disulfide (TMTD) semiultra accelerators, phenyl-*b*-naphthyl amine (PBN) antioxidant, and sulfur (curing agent), were used. Composites of NBR with magnetite nanoparticles were prepared at ratios of 100/0, 90/10, 80/20, 70/30, and 60/40 (wt %) and were designated as F0, F10, F20, F30, and F40, respectively, where the numbers indicate the weight percentages of the magnetite in the composites. The compound formulations are given in Table I. The physical mixing of the NBR/magnetite composites were carried out with an open two-roll mill (150 × 300 mm^2) at room temperature at a rotor speed of 60 rpm and a nip gap of about 1 mm (Qingdao Guangyue Rubber Machinery Co., Ltd., Shandong, China). Subsequently, other ingredients, including the vulcanizing agent, were added to the composite during the roll-mixing process under identical conditions of time, temperature, and rotor speed. Mixing occurred for 40 min at a room temperature of 25°C. The optimum cure times at 155°C for the NBR/magnetite nanocomposites were determined from a Monsanto oscillating disc rheometer R-100 (Shimatzuo, Osaka, Japan). Vulcanization was conducted under a heating press (Karl Kolb, Germany) at a pressure of 400 kPa and a temperature of 155°C for 60 min. The vulcanized samples were then conditioned before testing (72 h of maturation at room temperature).

TABLE I
Mix Formulation Used for the Preparation of the Nanocomposites

Sample ingredient	F0	F10	F20	F30	F40
NBR	100	100	100	100	100
Fe_3O_4	0	10	20	30	40
Stearic acid	3	3	3	3	3
Zinc oxide	7	7	7	7	7
DOP	1	1	1	1	1
MBTS	2	2	2	2	2
TMTD	1	1	1	1	1
PBN	1	1	1	1	1
Sulfur	1.75	1.75	1.75	1.75	1.75

All values are expressed as parts per hundred resin by weight.

Characterization and measurement techniques

Identification of the phase was carried out in the as-synthesized magnetite with an X-ray powder diffractometer (XRD). The X-ray diffractograms of these powder samples were recorded on a Philips

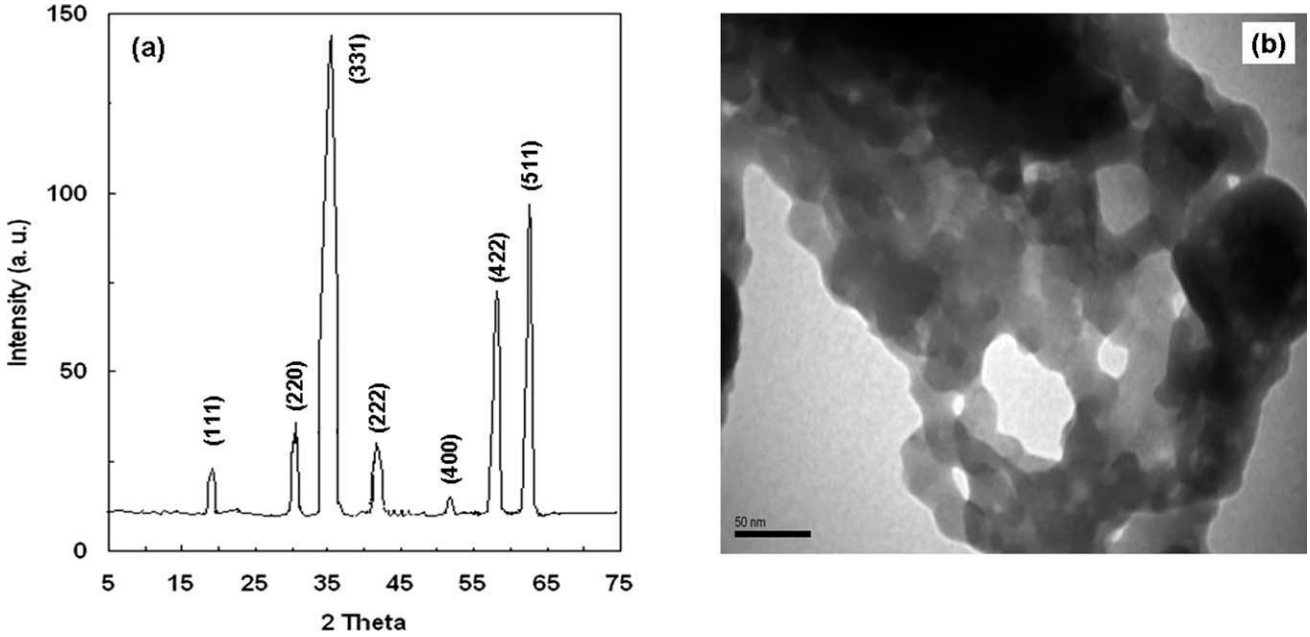

Figure 1 (a) X-ray diffraction pattern and (b) TEM of the as-synthesized magnetite (Fe_3O_4) nanoparticles.

(PW1130, Tokyo, Japan) X-ray diffractometer with Cu Kα radiation (λ = 0.1541 nm).

Transmission electron photographs of the as-prepared magnetite nanoparticles were obtained from a Philips CM 12 transmission electron microscope with an accelerating voltage 50 kV.

Field emission scanning electron micrographs were examined with a JEOL 4000 EX scanning microscope (JEOL, Tokyo, Japan) to study the morphology of the samples and quality of dispersion. The surfaces of the samples were mounted on aluminum studs with adhesive copper tape and were sputter-coated with gold before analysis. The chemical composition was measured by energy-dispersive X-ray spectroscopy (EDX; EDAX, Inc.). The density of the samples were measured by the Archimedes technique.[1] The mechanical properties, including the tensile strength (TS) and elongation at break (EB), were measured at room temperature with a material tester (AMETEK), which was connected by a digital force gage (Hunter Spring ACCU Force II, 0.01 N resolution), to measure the stress forces according to ASTM D 638. The force gage was interfaced with a computer to record the obtained data. The samples were in the form of strips (length = 2 cm, width = 2 mm, thickness = 1.1 mm). The Shore A hardness (*H*) was determined with a universal testing machine (ASTM D 2240 78, Kyowa Machinery Co LTD, Aichi, Japan). The room-temperature electrical conductivity was measured with the standard two-probe technique with parallel indium contacts. Data were collected with a digital multimeter (Keithley 642). The Ohmic behavior was checked in each case. The samples were in the form of discs with a cross-sectional area of 1 × 10^{-4} m^2 and a height of 1.4 mm. The carrier concentration and Hall mobility were estimated by Hall effect measurements with an alternating-current magnetic field of about 1 kG modulation with the van der Pauw configuration. The dielectric properties of the composites were measured at a frequency 1 kHz with an resistance, inductive and capacitive (RLC) measuring bridge (3541 Y-Hitester, Hioki, Japan). Silver paste was used to ensure good contact of the sample surface with the copper electrodes. EMI shielding effectiveness (SE) measurements were carried out with a Hewlett-Packard waveguide line containing a spectroanalyzer, power meter, coefficient of reflection meter, and coefficient of attenuation meter. Samples with a thickness of 2 mm were used during the measurements. The EMI shielding measurement was carried out for each sample by continuous sweeping of the frequencies between 1 and 12 GHz.

RESULTS AND DISCUSSION

Morphological and structural observations

To obtain the phase identification and composition, the X-ray diffraction spectrum of the as-synthesized magnetite (Fe_3O_4) nanoparticles is depicted in Figure 1(a). All peaks marked by their indices, (111), (220), (331), (222), (400), (422) and (511), could be assigned to the cubic spinel structure of magnetite and matched well with those of magnetite (ICSD no. 88–0315). It was clear that the particles were highly crystallized in a face-centered cubic structure. We also observed that the patterns exhibited broad peaks because of the small-size magnetite nanoparticles.

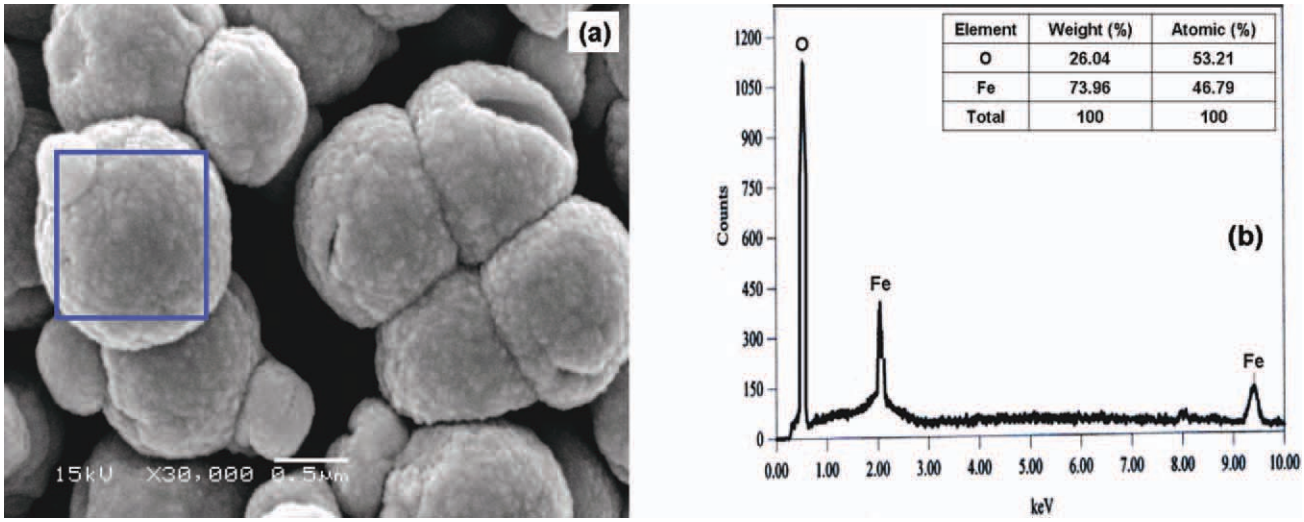

Figure 2 (a) Typical field emission scanning electron micrographs and (b) typical EDX spectra of the as-synthesized magnetite nanoparticles. [Color figure can be viewed in the online issue, which is available at wileyonlinelibrary.com.]

The calculated lattice parameter by least-squares fit was $a = 8.367$ Å. The average particle size (D) of the magnetite was quantitatively estimated with the well-known Scherrer formula:

$$D = \left(\frac{k\lambda}{\beta \cos\theta}\right)$$

where θ is the X-ray diffraction angle, k is the Debye–Scherrer constant (0.89) and is related to the particle shape and crystalline plane, β is the line broadening (rad) obtained from the full width at half-maximum of the diffraction peak, and λ is the X-ray wavelength (0.15406 nm). According to the Debye–Scherrer equation, the computed average particle size of the synthesized magnetite was 6 nm.

A typical transmission electron microscopy (TEM) micrograph of the as-synthesized magnetite is depicted in Figure 1(b). The TEM studies indicated that the magnetite particles were of nanometer size. They were approximately spherical in shape and monodisperse, with average diameters in the range 6–8 nm, which matched well those obtained from X-ray diffraction.

A field emission scanning electron microscope image of the as-synthesized magnetite nanoparticles is depicted in Figure 2(a). It was clear that all of the magnetite particles were spherical in nature, with diameters in the range 6–8 nm, and polydisperse.[1] In addition, the magnetite nanoparticles were highly aggregated because of the interactions between particles.

To confirm the formation of magnetite nanoparticles and determine their chemical composition, EDX analysis was carried out on the regime with the rectangle symbol in the left-field emission scanning electron microscopy image shown in Figure 2(a). Figure 2(b) is an EDX spectrum of the synthesized magnetite nanoparticles. It can be seen clearly in Figure 2(b) that strong peaks for iron (Fe) and oxygen (O) were observed; this indicated the formation of magnetite nanoparticles. The data of atomic weight of the as-synthesized magnetite were recorded in the table inset in Figure 2(b). We found that the atomic ratio of Fe to O was 1 : 1.37; this matched well that of magnetite. It is interesting to note that with random selection of the analytical regimes of the samples, we obtained similar results.

However, magnetite dispersion in the NBR matrix affected the final nanocomposite properties; therefore, it was necessary to investigate and quantify the dispersion of magnetite in the entire composites. The field emission scanning electron microscopy of composites containing 10 and 40 wt % magnetite, namely, samples F10 and F40, are depicted in Figure 3(a,b), respectively. In Figure 3(a), that is, sample F10, it is shown that a few crannies and some smaller holes were also observed, possibly because of the poor consistency between NBR and the magnetite nanoparticles, which resulted in phase separation to some extent. On the other hand, in Figure 3(b), that is, sample F40, it is shown that the magnetite nanoparticles were uniformly distributed throughout the NBR matrix. There was no obvious aggregation of magnetite nanoparticles in the nanocomposites. With increasing magnetite content, the packing of the particles grew denser. Moreover, this image confirms the excellent adhesion between the NBR matrix and the magnetite nanoparticles, and the good dispersion of conductive magnetite nanoparticles improved the electrical conductivity and shielding efficiency of the nanocomposite, as confirmed later in this article.

To gain a deeper insight into the influence of the magnetite content on the network structure, the number of elastically effective chains (NEC) of the

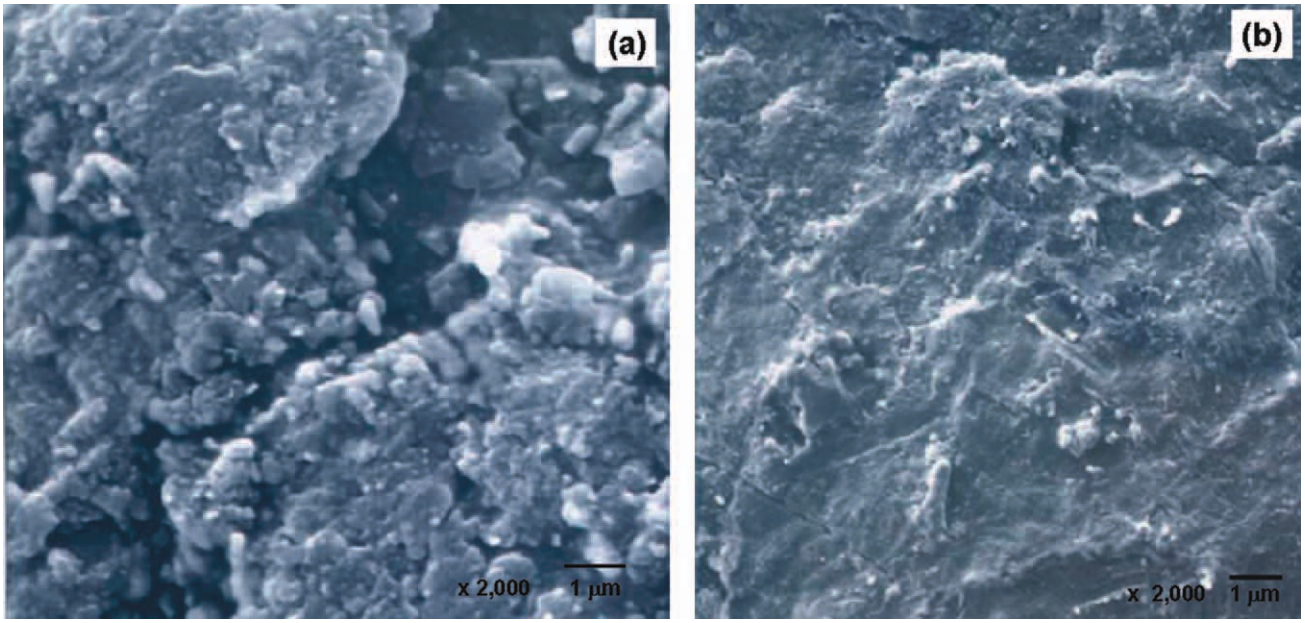

Figure 3 Typical field emission scanning electron micrographs of samples (a) F10 and (b) F40.

nanocomposites was estimated on the basis of the equilibrium swelling with the Flory–Rehner relation:[1,5]

$$\mathrm{NEC} = \frac{\rho_c N_A}{M_a} \tag{1}$$

where ρ_c is the composite density measured by the Archimedes method, N_A is Avogadro's number, and M_a is the average molecular weight of polymer crosslinks, which was computed by the following equation:[3,7]

$$M_a = -\frac{\rho_c V_s V_f^{1/3}}{\ln(1 - V_f) + V_{rf} + \chi V_f^2} \tag{2}$$

where V_s is the molar volume of the solvent (toluene), V_{rf} is the volume fraction of magnetite in nanocomposite, and χ is the Flory–Huggins interaction parameter between solvent and rubber, which is given by[5]

$$\chi = \theta + \frac{V_s\left(\beta_s - \beta_p\right)^2}{RT} \tag{3}$$

where θ is the lattice constant, β_s and β_p are the solubility parameters of the solvent and NBR polymer, respectively, R is the universal gas constant, T is the temperature (K), and V_f is the volume fraction of the rubber network in the solvent-swollen filled sample, estimated from the equilibrium swelling data as follows:[1]

$$V_f = \frac{\left(d - \phi_f w_0\right)\rho_p^{-1}}{\left(d - \phi_f w_0\right)\rho_p^{-1} + A_s \rho_s} \tag{4}$$

where d is the deswollen weight of sample, w_0 is the initial weight of the sample, ϕ_f is the volume fraction of magnetite, A_s is the amount of solvent absorbed by the sample, ρ_s is the density of the solvent, and ρ_p is the density of the polymer.

The polymer–filler interaction parameter (m) is given by[1,2]

$$\frac{V_{r0}}{V_f} = 1 - m\left(\frac{\phi_f}{1 - \phi_f}\right) \tag{5}$$

where V_{r0} is the volume fraction of the pure NBR polymer vulcanizates.

The interparticle distance between conductive chains (IPD) is given by the following equation:[6]

$$\mathrm{IPD} = \left(\frac{\pi D^3}{6\phi_f}\right)^{1/3} - D \tag{6}$$

where D is the diameter of the magnetite particles.

The computed values of NEC, V_f, m, and IPD of the nanocomposites as a function of the magnetite content are depicted in Figure 4. It was observed that NEC, V_f, and m increased with increasing magnetite content in the nanocomposites. The augmentation of NEC could be attributed to the fact that the magnetite nanoparticles favored the formation of an effective chains network across the NBR matrix and formed more linked branches within the composite network. Also, it was observed that V_f increased with increasing magnetite nanoparticle content. This indicated that the magnetite nanoparticles had better

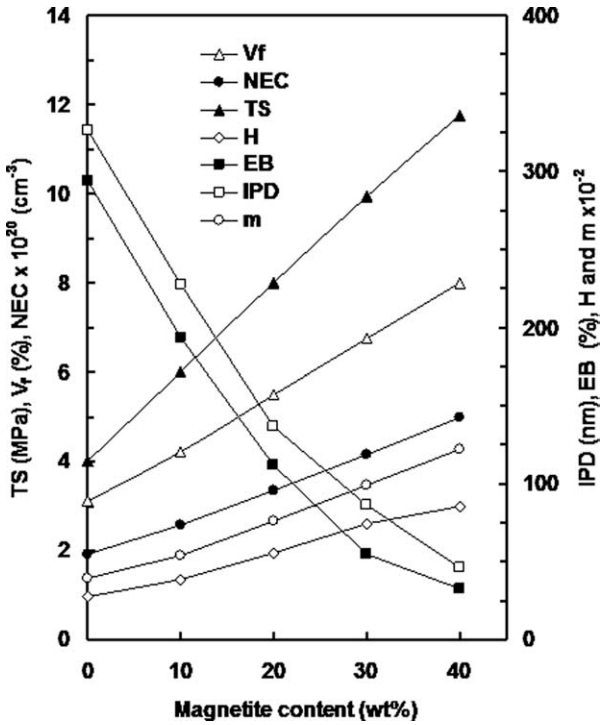

Figure 4 TS, EB, *H*, IPD, NEC, volume fraction of rubber (V_r), and *m* versus magnetite weight content for the composites.

adhesion, and there was a higher extent of interaction between the magnetite particles and the NBR matrix. It was observed that the *m* values increased with increasing magnetite content in the composites, as shown in Figure 4. This supported the fact that the inclusion of magnetite particles improved the molecular structure and increased the excluded volume (i.e., the molecular connectivity) of the composites. The relationship between IPD and the magnetite content is also presented in Figure 4. As expected, IPD decreased with increasing magnetite content in the composites. The observed trend was the result of the intermolecular distance decrease and the crosslinking density increase with increasing magnetite loading level in the composites. This led to the electron hopping increase resulting in an increase in the whole composite electrical conductivity, as confirmed later in this article.

Again, to better understand the effect of magnetite nanoparticles on the network structure, the mechanical properties of the NBR/magnetite nanocomposites were measured. The variation of TS, EB, and *H* of NBR/magnetite nanocomposites as a function of the magnetite content is depicted in Figure 4. In Figure 4, it is clear that the hardness increased with increasing magnetite content in the composites. This was due to strong bonding between the NBR polymer matrix and the magnetite nanoparticles, which tended to restrict the chain mobility and, again, resulted in an increase in the hardness for the composite samples. It is well known that the hardness is directly related to the TS of a material. It can be seen in Figure 4 that the presence of magnetite nanoparticles considerably increased the TS of the NBR/magnetite nanocomposites. The improved TS with magnetite content could be ascribed to the improved interfaces between the magnetite nanoparticles and the crosslinked NBR matrix. This showed that the magnetite nanoparticles effectively played their role as a reinforcement and rendered good mechanical properties to the NBR polymer matrix. Furthermore, the magnetite nanoparticles improved the interfacial adhesion and yielded greater strength in the composites. The interfacial bonding facilitated efficient stress transfer between the magnetite nanoparticles and the NBR polymer matrix and led to an improved reinforcing effect.[9] EB decreased with increasing content of magnetite nanoparticles in the NBR/magnetite nanocomposites. This implied that the ductility of the NBR matrix was effectively improved by the incorporation of magnetite nanoparticles in the nanocomposites. The magnetite nanoparticles were expected to act as bridges to prolong the fracture process of the NBR/magnetite nanocomposites. A strong interfacial adhesion between the NBR matrix and the magnetite nanoparticles reduced the polymer mobility and prevented magnetite nanoparticle pullouts from the NBR matrix. Furthermore, the decrease in EB was attributed to the enhancement of interactions between the NBR matrix and the magnetite nanoparticles, which limited the segmental movement of the NBR matrix.

Static electrical properties

The room-temperature, direct-current volume electrical conductivity, mobility carriers (μ), and number of charge carriers per unit volume (*N*) of the NBR/magnetite nanocomposites are depicted in Figure 5. It can be found in Figure 5 that the NBR/magnetite nanocomposites exhibited a typical percolation behavior, and the introduction of magnetite nanoparticles into the NBR matrix increased the conductivity of the resulting composites by several orders of magnitude or by even higher than seven orders of magnitude. The measured room-temperature conductivity of the pure NBR was 1.3×10^{-10} S/cm.[2,10] It was seen that for a weight fraction of magnetite below 2 wt %, the composites were almost isolated, and the conductivity was governed by the electrical characteristics of the base NBR polymer matrix. As the weight fraction of magnetite increased further, the gap width among the conductive phases became sufficiently small for electrons to tunnel or hop through the NBR matrix or for interface contact between magnetite and NBR matrix.

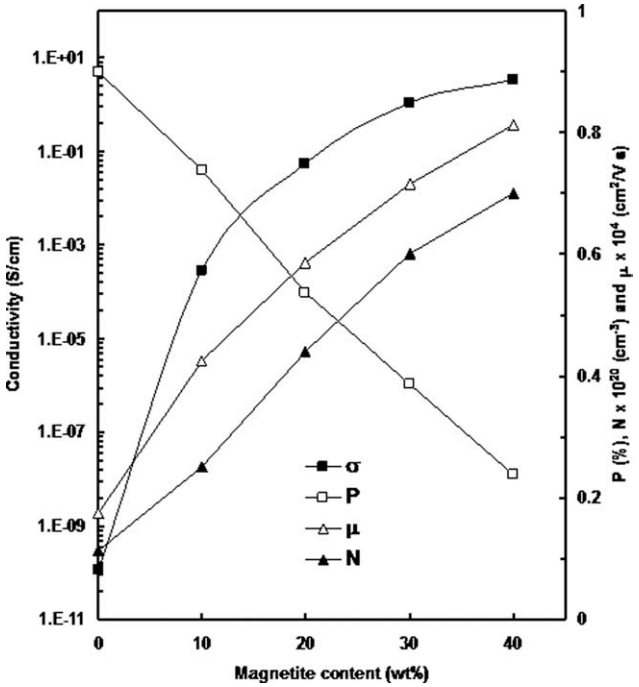

Figure 5 Variation of the volume electrical conductivity, (μ), N, and porosity of the composites with magnetite weight content.

Statistical percolation theory was applied to explain the behavior of the electrical conductivity (σ) and to determine the percolation threshold concentration of the NBR/magnetite nanocomposites. This was described by a power law of the following form:[4,11]

$$\sigma = \sigma_0\left(\phi_f - \phi_c\right)^S \tag{7}$$

where σ_0 is the electrical conductivity of the magnetite nanoparticles, ϕ_c is the critical volume fraction at which percolation takes place, and S is the critical exponent of conductivity, which reveals the lattice dimensionality.

A best fit of the conductivity data to the log–log plots of power law gives $\phi_c = 2$ wt % and $S = 2.89$. It is interesting to note that the low value of the percolation threshold was due to the high surface area of magnetite nanoparticles and good interfacial contact between NBR and the magnetite nanoparticles. The high value of the critical exponent was ascribed to the good dispersion of the magnetite nanoparticles and increase in NEC inside the nanocomposites. In closing, the magnetite nanoparticles were dispersed in the entire composites in a three-dimensional network structure; this led to a higher electrical conductivity of the composites and a better EMI SE of the composites, as confirmed later in this study.[12] This may have been due to the formation of a conductive network or electrical mesh within the NBR matrix. In addition, above this critical concentration, the change in conductivity with magnetite loading was only marginal; hence, this loading was the optimum choice for effective shielding for these composites. Therefore, any further increase in the magnetite weight content would only improve the resulting electromagnetic characteristics.

Also, in Figure 5, it was observed that μ_m and N increased with increasing magnetite loading level in the composites. There were two possible reasons for the increases in both μ_m and N with increasing magnetite content in the composites. First was the increase in the interfacial adhesion between the magnetite and NBR matrix, which accelerated the driving force of the transport of the charge carriers. Second, with increasing magnetite, the vacant volume between the conductive sites decreased; this led to an increase in the hopping or tunneling of the charge carriers and increased the density of electrical mesh and/or magnetite particles interconnected within the NBR matrix. This was a strong clue that the inclusion of magnetite in the NBR matrix acted as a carrier reservoir for the entire composite.

Again, to confirm these facts, we evaluated the porosity (P) of the NBR/magnetite nanocomposites by using the following equation:[2,13]

$$P = \frac{\rho_{\text{th}} - \rho_{\text{exp}}}{\rho_{\text{th}}} \tag{8}$$

where ρ_{exp} and ρ_{th} are the experimental and theoretical densities of the composites. ρ_{th} is given by the following expression:

$$\rho_{\text{th}} = \rho_f\phi_f + \left(1 - \phi_f\right)\rho_m \tag{9}$$

where ρ_f is the density of magnetite and ρ_m is the density of the NBR polymer matrix.

The computed values of the porosity as a function of magnetite loading are depicted in Figure 5. It was clear that the porosity decreased with increasing magnetite content in the composites. This reflected the fact that the void content among the conductive sites decreased, and the formation of an interconducting network of magnetite nanoparticles increased in the NBR matrix. This led to the transport of charge carriers in the entire composite.

SE of EMI

An electromagnetic shielding material is a material that attenuates radiated electromagnetic energy.[13] SE is typically measured as an attenuation of the electromagnetic signal after a shield is introduced, that is, how much the EMI emission energy has been reduced. Thus, attenuation is a measure of the reduction in the intensity of the electromagnetic field

and is normally reported in decibels. SE is a number that quantifies the amount of attenuation typical of a particular material at a specific frequency and can be expressed by the following equation:[2,13]

$$\mathrm{SE} = 10\log\left(\frac{P_I}{P_T}\right) = 20\log\left(\frac{E_I}{E_T}\right) = 20\log\left(\frac{H_I}{H_T}\right) \quad (10)$$

where P_I, E_I, and H_I are the power and the electric and magnetic field intensities incident on the shield and P_T, E_T, and H_T are the counterparts transmitted through the shield, respectively.

However, the SE or insertion loss represents the reduction of the level of an electromagnetic field at a point in space after a conductive specimen is inserted between that point and the source. SE is described as the algebraic sum of the contributions due to the reflection loss (SE_R), transmittance or absorbance loss, and internal reflection loss and are interrelated by[13,14]

$$\mathrm{SE} = \mathrm{SE}_R + \mathrm{SE}_A + \mathrm{SE}_M \quad (11)$$

where SE_A is the absorption loss and is known as the energy dissipation due to the interaction of electromagnetic irradiation with the material, SE_R is due to the impedance mismatch between air and the material at the measured frequency, and SE_M is the internal reflection due to the inhomogeneity of the entire material.

For plane-wave radiation, SE_A and SE_R may be calculated from the following equations:[15]

$$\mathrm{SE}_A = 3.32h\sqrt{f\mu_r\sigma_r} \quad (12)$$

$$\mathrm{SE}_R = 108 + \log\left(\frac{\sigma_r}{f\mu_r}\right) \quad (13)$$

where h is the thickness of the tested specimen, f is the incident frequency, σ_r is the conductivity of the specimen relative to copper (conductivity of copper $\approx 5.82 \times 10^5$ S/cm), and μ_r is the permeability relative to copper or the vacuum and is taken to be 1. In fact, electromagnetic radiation at high frequencies penetrates only near the surface region of an electrical conductor. This is known as the *skin effect*. The electric field of a plane wave penetrating a conductor drops exponentially with increasing depth in the conductor.[16] The depth at which the field drops to $1/e$ of the incident value is called the *skin depth* (δ). With these considerations, the SE depends on the relative value of the thickness of the sample with regard to δ and is defined by[10]

$$\delta = \frac{1}{\sqrt{\pi f\mu_r\mu_0\sigma_r}} \quad (14)$$

where μ_0 is the absolute permeability of free space (air) and is equal to $4\pi \times 10^{-7}$ H/m.

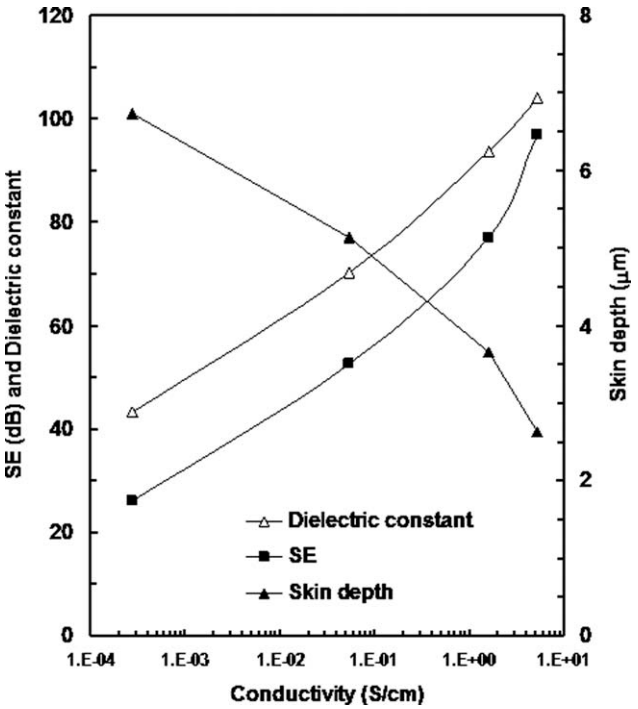

Figure 6 EMI SE, δ, and dielectric constant versus conductivity of the composites.

The variations of the δ, dielectric constant, and EMI SE of the NBR/magnetite nanocomposites as a function of the conductivity of the nanocomposites are depicted in Figure 6. As expected, δ decreased with increasing electrical conductivity of the NBR/magnetite nanocomposites. This was due to the increase of the crosslinking density with increasing magnetite content in the composites.[3] This indicated that the multireflections contributed to the total SE of the NBR/magnetite nanocomposites.[9] It is shown in Figure 6 that an increase in the amount of magnetite nanoparticles increased the number of magnetite nanoparticles in the nanocomposites interacting with incident radiation and caused SE to increase in the nanocomposites. This was attributed to the increases in the interfacial adhesion and charge carriers of the composites. In addition, the high SE of NBR/magnetite was attributed to the small diameter and high absorbability of the magnetite nanoparticles. It is worth noting that the ferromagnetic properties of magnetite also helped to enhance SE of the nanocomposites. It is shown in this figure that the dielectric constant increased gradually with increasing magnetite content in the nanocomposites. The dielectric constant had contributions from the orientation, atomic, and electronic polarizations and was affected by a factors such as the interfacial adhesion among the filler and matrix, porosity, volume fraction of the filler, and the number of mobile charge carriers in the composites.[11] As the magnetite loading increased, the connectivity among the magnetite nanoparticle increased; this led

to an increase in the dipole–dipole interaction. In addition, the increase of magnetite nanoparticles increased the interface zone between magnetite and the NBR matrix and decreased the voids inside the composites. The increase in the dielectric constant with increasing magnetite content was interpreted by the increase of the interfacial polarization and the decrease in porosity in the nanocomposites. In addition, the increase in the dielectric constant was due to the increase in the number of dipole moments in the entire composites. This led to an increase in the orientation polarization.

For practical applications of NBR/magnetite nanocomposites as electromagnetic shielding devices, it is necessary to monitor the variation of SE with the applied frequency. The variation of the experimental SE of different compositions of magnetite reinforced in the NBR matrix over the frequency range 1–12 GHz is displayed in Figure 7. Figure 7 shows that the SE of the nanocomposites was increased effectively with the magnetite content over the frequency range 1–12 GHz. It was observed that SE increased with increasing frequency, as expected. As the frequency increased, the wavelength of the electromagnetic wave decreased and became closer to the size of the magnetite particles. Therefore, the higher frequency waves were more likely to encounter magnetite incorporated in the entire NBR matrix. It is interesting to note that there was an increase in SE with increasing magnetite content in the NBR matrix. Also, at higher contents, the composites became more efficient in shielding. This may have been due to the orientation of domains remaining perpendicular to the direction of wave propagation. Furthermore, magnetite exhibited conduction losses with additional magnetic losses, such as hysteresis, domain wall resonance, and electron spin resonance; this led to a higher shielding efficiency in the composites. This result suggests that the shielding efficiency was directly related to the number of conducting phases in the composites; this could have changed the conductivity and, consequently, the absorption of the incident radiation. The variation of the calculated SE of different compositions of magnetite reinforced in the NBR matrix over the frequency range 1–12 GHz is depicted in Figure 8. In comparison, it was seen that a good agreement was obtained between the measured and calculated SEs in the microwave frequency.

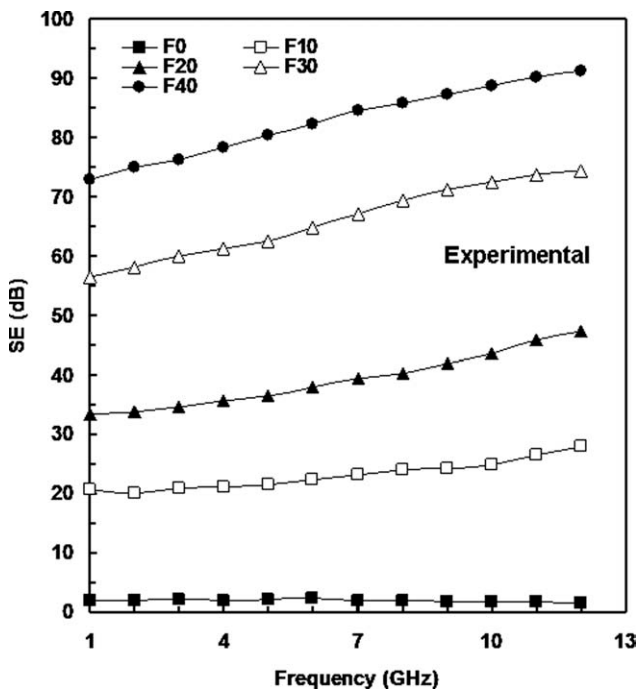

Figure 7 Measured EMI SE versus frequency for the NBR/magnetite nanocomposites.

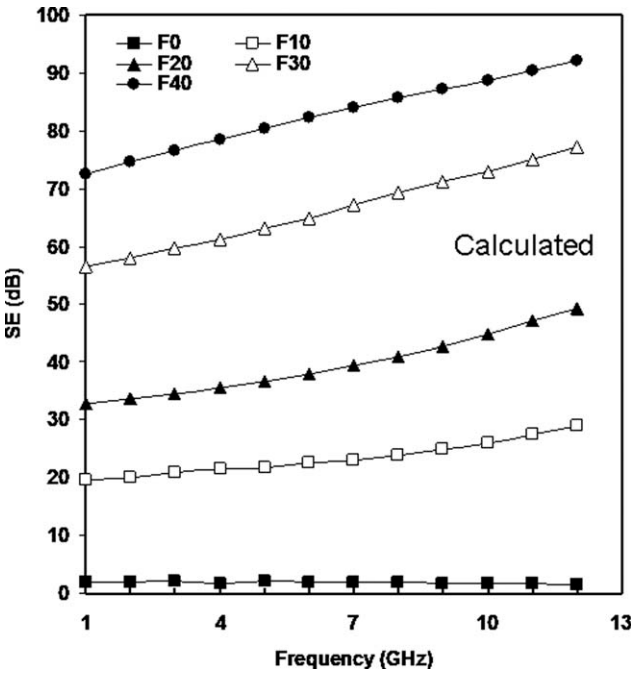

Figure 8 Calculated EMI SE versus frequency for the NBR/magnetite nanocomposites.

CONCLUSIONS

1. We successfully synthesized magnetite nanoparticles in a regular sphere with average diameters of about 6 nm via a hydrothermal route for the first time using a hexahydrate ($FeCl_3 \cdot 6H_2O$) source of iron, $Na_2C_2O_4$, and ethylene glycol.
2. The inclusion of magnetite nanoparticles to the NBR matrix improved the microstructure, NEC, and mechanical properties of the nanocomposites.
3. The electrical conductivity, μ, and number of charge carrier increased with increasing magnetite content in the composites. The electrical percolation threshold of the NBR/magnetite nanocomposite was only 2 wt % magnetite.

4. The observed EMI shielding revealed that the NBR/magnetite nanocomposite with higher magnetite contents (i.e., 40 wt %) had a greater EMI SE of about 92 dB over the frequency range 11–12 GHz. This was attributed to the higher electrical conductivity and fast spin relaxation of superparamagnetic particles distributed in the NBR polymer matrix.
5. This kind of composite material may find good applications in microwave absorption devices, such as absorbers of nonionizing electromagnetic waves, and can be used as functional fillers for the creation of such materials.

The present research is a result of an international collaboration program between University of Tabuk, Tabuk, Kingdom of Saudi Arabia and the University of Chemical Technology and Metallurgy, Sofia, Bulgaria. The authors gratefully acknowledge the financial support from the University of Tabuk.

References

1. Al-Ghamdi, A. A.; El-Tantawy, F. Compos A 2010, 41, 1693.
2. Al-Juaid, S. S.; El-Mossalamy, E. H.; Arafa, H. M.; Al-Ghamdi, A. A.; Abdel Daiem, A. M.; El-Tantawy, F. J Appl Polym Sci 2011, 121, 3604.
3. El-Tantawy, F.; Abdel Aal, N.; Sung, Y. K. Macromol Res 2005, 13, 194.
4. El-Tantawy, F.; Abdel-Kader, K. M.; Kaneko, F.; Sung, Y. K. Eur Polym J 2004, 40, 415.
5. Dhawan, S. K.; Singh, N.; Rodrigues, D. 2003, 4, 2105.
6. Liu, Z.; Bai, G.; Huang, Y.; Ma, Y.; Du, F.; Li, F. Carbon 2007, 45, 821.
7. Liu, Z.; Bai, G.; Huang, Y.; Li, F.; Ma, Y.; Guo, T.; He, X.; Lin, X.; Gao, H.; Chen, Y. J Phys Chem C 2007, 111, 13696.
8. Keith, J. M.; Janda, N. B.; King, J. A. Polym Compos 2005, 5, 671.
9. Klemperer, C. J.; Maharaj, D. Compos Struct 2009, 91, 467.
10. Al-Saleh, M. H.; Gelves, G. A.; Sundararaj, U. Compos A 2011, 42, 92.
11. Hoang, N. H.; Wojkiewicz, J. L.; Miane, J. L.; Biscarro, R. S. Polym Adv Technol 2007, 18, 257.
12. Al-Saleh, M. H.; Sundararaj, U. Carbon 2009, 47, 1738.
13. Das, N. C.; Chaki, T. K.; Khastgir, D. Adv Polym Technol 2001, 20, 226.
14. Koysuren, O.; Yesil, S.; Bayram, G.; Secmen, M.; Civi, O. A. J Appl Polym Sci 2008, 109, 152.
15. Hoang, N. H.; Wojkiewicz, J. L.; Miane, J. L.; Biscarro, R. S. Polym Adv Technol 2007, 18, 257.
16. Das, N. C.; Liu, Y.; Yang, K.; Peng, W.; Maiti, S.; Wang, H. Polym Eng Sci 2009, 49, 29.